



HAL
open science

Control Theory and Fast Marching Methods for Brain Connectivity Mapping

Emmanuel Prados, Christophe Lenglet, Jean-Philippe Pons, Nicolas Wotawa, Rachid Deriche, Olivier Faugeras, Stefano Soatto

► **To cite this version:**

Emmanuel Prados, Christophe Lenglet, Jean-Philippe Pons, Nicolas Wotawa, Rachid Deriche, et al.. Control Theory and Fast Marching Methods for Brain Connectivity Mapping. [Research Report] RR-5845, INRIA. 2006, pp.21. inria-00070181

HAL Id: inria-00070181

<https://inria.hal.science/inria-00070181>

Submitted on 19 May 2006

HAL is a multi-disciplinary open access archive for the deposit and dissemination of scientific research documents, whether they are published or not. The documents may come from teaching and research institutions in France or abroad, or from public or private research centers.

L'archive ouverte pluridisciplinaire **HAL**, est destinée au dépôt et à la diffusion de documents scientifiques de niveau recherche, publiés ou non, émanant des établissements d'enseignement et de recherche français ou étrangers, des laboratoires publics ou privés.



INSTITUT NATIONAL DE RECHERCHE EN INFORMATIQUE ET EN AUTOMATIQUE

*Control Theory and Fast Marching Methods
for Brain Connectivity Mapping*

Emmanuel Prados — Christophe Lenglet — Jean-Philippe Pons — Nicolas Wotawa —
Rachid Deriche — Olivier Faugeras — Stefano Soatto

N° 5845

February 17, 2006

Thème BIO



*R*apport
de recherche

Control Theory and Fast Marching Methods for Brain Connectivity Mapping

Emmanuel Prados^{*}, Christophe Lenglet[†], Jean-Philippe Pons[†], Nicolas
Wotawa[†], Rachid Deriche[†], Olivier Faugeras[†], Stefano Soatto[‡]

Thème BIO — Systèmes biologiques
Projet Odysée

Rapport de recherche n° 5845 — February 17, 2006 — 21 pages

Abstract: We propose a novel, fast and robust technique for the computation of anatomical connectivity in the brain. Our approach exploits the information provided by Diffusion Tensor Magnetic Resonance Imaging (or DTI) and models the white matter by using Riemannian geometry and control theory. We show that it is possible, from a region of interest, to compute the geodesic distance to any other point and the associated optimal vector field. The latter can be used to trace shortest paths coinciding with neural fiber bundles. We also demonstrate that no explicit computation of those 3D curves is necessary to assess the degree of connectivity of the region of interest with the rest of the brain. We finally introduce a general local connectivity measure whose statistics along the optimal paths may be used to evaluate the degree of connectivity of any pair of voxels. All those quantities can be computed *simultaneously* in a Fast Marching framework, directly yielding the connectivity maps. Apart from being extremely fast, this method has other advantages such as the strict respect of the convoluted geometry of white matter, the fact that it is parameter-free, and its robustness to noise. We illustrate our technique by showing results on real and synthetic datasets. Our **GCM** (Geodesic Connectivity Mapping) algorithm is implemented in C++ and will be soon available on the web.

Key-words: Control Theory, Fast Marching Methods, PDE, Riemannian Manifold, Hamilton-Jacobi-Bellman equations, Brain Connectivity Mapping, connectivity measures

* UCLA Vision Lab., USA

† Odysée Lab., INRIA Sophia Antipolis, France

‡ UCLA Vision Lab., USA

Théorie du Contrôle et Méthodes de Fast Marching pour l'Étude de la Connectivité Cérébrale

Résumé : Nous présentons une technique originale, rapide et robuste pour l'estimation de la connectivité anatomique cérébrale. Notre approche exploite l'information fournie par l'IRM du tenseur de diffusion et modélise la matière blanche sur la base d'outils empruntés à la géométrie Riemannienne et à la théorie du contrôle. Nous montrons qu'il est possible, à partir d'une région d'intérêt, de calculer la distance géodésique à tout autre point, ainsi que le champ de vecteur optimal associé. Ce dernier peut être utilisé pour retrouver les plus courts chemins coïncidants avec les fibres nerveuses. Nous montrons également que le calcul explicite de ces courbes 3D n'est en fait pas nécessaire pour évaluer le degré de connectivité de la région d'intérêt avec le reste du cerveau. Nous introduisons enfin une mesure de connectivité locale générale dont les statistiques le long des chemins optimaux peuvent être utilisées pour évaluer le degré de connectivité entre deux voxels. Toutes ces quantités peuvent être calculées *simultanément* par un balayage de type "Fast Marching", conduisant ainsi directement aux cartes de connectivité. Cette méthode n'est pas seulement extrêmement rapide mais présente aussi d'autres avantages tels que le strict respect de la géométrie convoluée de la matière blanche, l'absence totale de paramètre, et une grande robustesse au bruit. Nous illustrons notre technique sur des données réelles et synthétiques. Notre algorithme (appelé **GCM** pour "Geodesic Connectivity Mapping") et implémenté en C++ et sera très prochainement disponible sur le web.

Mots-clés : Théorie du contrôle, Méthodes de "Fast Marching", EDP, variété Riemannienne, équations de Hamilton-Jacobi-Bellman, cartographie de la connectivité cérébrale, mesures de connectivité

Contents

| | | |
|----------|---|-----------|
| 1 | Introduction | 4 |
| 2 | From Geometry to Control Theory | 5 |
| 3 | Connectivity Measures | 7 |
| 4 | A Fast Numerical Algorithm | 8 |
| 4.1 | Related Work and Contributions | 8 |
| 4.2 | Global Algorithm | 10 |
| 4.3 | Distance and Optimal Dynamics Computation | 10 |
| 4.3.1 | Separation and choice of the good simplex | 10 |
| 4.3.2 | Computation of t_s and of the associated dynamics | 11 |
| 4.3.3 | Details for the 3D-anisotropic eikonal equation | 12 |
| 4.4 | Connectivity Measures Computation | 12 |
| 5 | Experimental Results | 13 |
| 5.1 | Challenging Computational Issues | 13 |
| 5.1.1 | Handling the white matter convoluted geometry | 14 |
| 5.1.2 | Robust estimation of the optimal dynamics | 14 |
| 5.2 | Fast and Robust Anatomical Connectivity Measure | 14 |
| 5.2.1 | Data acquisition | 15 |
| 5.2.2 | Computational efficiency | 15 |
| 5.2.3 | Performance of the connectivity measure | 17 |
| 6 | Conclusion | 18 |

1 Introduction

Diffusion magnetic resonance imaging [7] is a technique to characterize the anisotropic diffusion of water molecules in structured biological tissues. As of today, it is the only non-invasive method that allows to distinguish the anatomical structures within the cerebral white matter. Diffusion tensor (DT) imaging [4] models the probability density function of the three-dimensional molecular motion, at each voxel of a DT image, by a local Gaussian process whose covariance matrix is precisely given by the diffusion tensor. Among other applications, diffusion tensor imaging (DTI) is extremely useful to estimate the anatomical connectivity of the human brain.

Following [20], various local approaches have already been proposed to tackle this problem. They are based on line propagation techniques and rely on the fact that the eigenvector of the diffusion tensor associated to the major eigenvalue, provides a relatively accurate estimate of the fibers' orientation at each voxel. These methods may be refined to incorporate some natural constraints such as regularity or local uncertainty and avoid being stopped in regions of low anisotropy [5, 35, 8, 14, 17]. All these efforts aim to overcome the intrinsic ambiguity of diffusion tensor data arising from partial volume effects at locations of fiber crossings [2]. They provide relatively accurate models of the white matter macroscopic bundles.

Most recent work can be divided into approaches based on Bayesian models and geometric methods, the latter essentially based on front-propagation techniques. They are both more robust to noise and partial volume effects than previous work, and naturally yield probability/scalar measures which can be used to evaluate the degree of connectivity between voxels. In [6, 23, 13] stochastic tractography algorithms were introduced by modeling the uncertainty of the local fiber orientation. Through uncertainty propagation, they provide a powerful means to evaluate the probability of connection between points of the white matter. However, the intrinsic drawback of these methods is their computational complexity since it is necessary to resort to Markov Chain Monte Carlo methods or, as in [13], to evaluate probability density functions at enough locations of the space of interest.

Geometric methods use either Level Set methods [21, 18, 22], Fast Marching methods [24, 34, 30] or iterative sweeping techniques [15] to evolve a front on the basis of the diffusion tensor directional information. As described in [9], it is possible to adapt the Level Set-based front propagation technique to take advantage of the information provided by high angular resolution diffusion MRI. However, this method tends to be somewhat inefficient since, even with a narrow-band implementation, the number of points where the evolution speed has to be evaluated greatly increases as the surface grows. We will also show that this class of methods is prone to interpolation errors at the boundary of the domain. For our brain connectivity problem, this may lead to erroneous connections in highly convoluted areas.

Our contribution is threefold: First of all, on the basis of [18], we propose to efficiently and robustly estimate the anatomical connections of the white matter as geodesics in \mathbb{R}^3 equipped with a Riemannian metric derived from the diffusion tensor. We demonstrate that it is possible to solve,

quickly and simultaneously, for the geodesic distance, the optimal vector field (optimal dynamics) corresponding to the geodesics velocities and the statistics, along those curves, of a local connectivity measure. To our knowledge, the proposed GCM algorithm is faster than any other existing method. Also, contrary to other approaches, we simply solve the anisotropic eikonal equation and do not resort to any anisotropy related parameter to constrain the front propagation. The second contribution is the ability of the algorithm to work within a mask of the white matter accurately obtained by segmentation of a high-resolution anatomical MRI. As we will show, this is crucial for the application of interest since we must strictly respect the geometry of the cortical foldings or white matter / cerebrospinal fluid (CSF) interface to recover meaningful connections. To our knowledge this technical issue has never been addressed before. Finally, for a region of interest x_0 (i.e. a point of the white matter), our GCM method generates statistics of a local connectivity measure along the geodesics linking x_0 to other locations of the brain. This can be used to discriminate likely and unlikely connections.

2 From Geometry to Control Theory

In [21, 18], the problem is formulated in the framework of Riemannian geometry. The white matter is interpreted as a Riemannian manifold and the diffusion tensor provides the Riemannian metric, which in turn determines white matter fibers as geodesic paths. We remind the basic definition of geodesics for convenience [11].

Definition 2.1 (geodesics) *Let $(\mathcal{M}, |\cdot|_R)$ be a Riemannian manifold. Let $x, y \in \mathcal{M}$. The geodesic connecting x to y is the curve γ_0 which minimizes the arc length, i.e.*

$$\gamma_0 = \arg \min_{\gamma \in \Gamma_{x,y}} \int_0^{T_{xy}} |\gamma'(t)|_R dt$$

where $\Gamma_{x,y}$ is the set of curves $\gamma : [0, T_{xy}] \rightarrow \mathcal{M}$ such that $\gamma(0) = x$, $\gamma(T_{xy}) = y$ and $|\gamma'(t)|_R = 1$.

In [18], the authors show that the appropriate metric to our problem is the one associated to the norm $|\cdot|_R$ defined by $|x|_R = \sqrt{x^T D_x^{-1} x}$, where D_x is the symmetric positive definite 3×3 -matrix given by the measured diffusion tensor, i.e. the data. Let us also denote with A_x the (symmetric positive definite) square root matrix of D_x and with $|\cdot|_E$ the Euclidian norm. Let us note that we have trivially $|x|_R = |A_x^{-1} x|_E$.

Here, rather than interpreting the problem in terms of Riemannian geometry, we adopt an optimal control point of view. The two interpretations are equivalent, but focus on different aspects of the problem. In the Riemannian setting, the emphasis is on the description of the geometry and in particular on the geodesics. In the optimal control interpretation, the emphasis is on the optimal dynamics, i.e. the intrinsic gradient of the distance function or, in other words, the vector field tangent to the geodesics. Specifically, let a domain Ω be a subset of \mathbb{R}^3 representing the white matter. We consider the set \mathcal{A} (compact subset of \mathbb{R}^N) of admissible controls a ($a \in \mathcal{A}$), a target (here the point of interest x_0 , origin of the distance function), a vector field $f(x, a)$ (called *dynamics*) that depends on the control and a *cost* $l(x, a)$, $x \in \Omega$. We call *control function*, a function $\alpha(\cdot) : \Omega \rightarrow \mathcal{A}$. Under some regularity assumptions, to each control function α and $x \in \Omega$, we can

associate a single trajectory $\xi_{x,\alpha}(t) \in \Omega$ following the dynamics $\xi'(t) = f(\xi(t), \alpha(\xi(t)))$, $t > 0$, imposed by the control α , see [3]. Moreover, one can prove that there exists a control function α^* (the *optimal control*) such that for all x , the integral of the cost along the associated trajectory ξ_{x,α^*} is minimal [3]. We then denote by $\xi_x^* \stackrel{\text{def}}{=} \xi_{x,\alpha^*}$ the *optimal trajectory* starting from x and $f_x^* \stackrel{\text{def}}{=} f(x, \alpha^*(x))$ the optimal dynamics at x . The goal is to characterize and compute this optimal control α^* (f_x^* being immediately deduced from α^*).

If we let $l(x, a) = 1$, then the problem consists in finding the control function α^* s.t. for all x in Ω and for all α

$$\int_0^{T_{x,x_0,\alpha^*}} l(\xi_{x,\alpha^*}(t), \alpha^*(\xi_{x,\alpha^*}(t))) dt \leq \int_0^{T_{x,x_0,\alpha}} l(\xi_{x,\alpha}(t), \alpha(\xi_{x,\alpha}(t))) dt,$$

i.e.

$$T_{x,x_0,\alpha^*} \leq T_{x,x_0,\alpha},$$

where $T_{x,x_0,\alpha}$ is the first time for which the trajectory $\xi_{x,\alpha}$ (controlled by the dynamics f) reaches the target x_0 . $T_{x,x_0,\alpha} = +\infty$ if the trajectory does not reach x_0 . In other words (misusing the notations) α^* is

$$\alpha^* = \arg \min_{\alpha(\cdot)} \left\{ \int_0^{T_{x,x_0,\alpha}} l(\xi(t), \alpha(\xi(t))) dt \right\} = \arg \min_{\alpha(\cdot)} \left\{ \int_0^{T_{x,x_0,\alpha}} 1 dt \right\} = \arg \min_{\alpha(\cdot)} \{T_{x,x_0,\alpha}\}. \quad (1)$$

If furthermore we let \mathcal{A} be the set of $A_x^T b$ for b in the Euclidian unit sphere (\mathcal{A} coincides then with the unit Riemannian sphere associated to A_x) and $f(x, a) = a$ (i.e. the dynamics is equal to the control), then we can see that in this case, the optimal trajectories ξ_x^* correspond to the geodesics considered in [18] (when α covers \mathcal{A} , $\xi'(t) = \alpha(\xi(t))$ also covers \mathcal{A}).

The control interpretation has distinct advantages: All the objects of interest live in \mathbb{R}^3 (instead of a manifold), and are governed by the Euclidian metric, hence the interpretation is independent of the geometric structure. As an illustration of this benefit, in order to estimate the direction of the geodesics, Lenglet et al. [18] proposed to compute the gradient of the distance function on the manifold, which requires some care in order to take into account the geometry imposed by the metric and is a challenging task when working on an irregular domain such as the brain white matter. In the control formalism the interpretation is rather direct: *the tangent of the geodesics is in fact the optimal dynamics f_x^** (since the geodesic corresponds to the optimal trajectories). Also, the optimal dynamics f_x^* coincides with the optimal control, which is the direct outcome of our algorithm. The control framework reveals the fact that the *value function* V defined by the min of equation (1)

$$V(x) = \min_{\alpha} \left\{ \int_0^{T_{x,x_0,\alpha}} l(\xi(t), \alpha(\xi(t))) dt \right\} = \min_{\alpha} \left\{ \int_0^{T_{x,x_0,\alpha}} 1 dt \right\} = \min_{\alpha} T_{x,x_0,\alpha} \quad (2)$$

is the viscosity solution of the partial differential equation (PDE)

$$\sup_{a \in \mathcal{A}} \{-f(x, a) \cdot \nabla u(x) - l(x, a)\} = 0, \quad (3)$$

verifying $u(x_0) = 0$ and complemented by state constraints on the boundary of the domain $\partial\Omega$ [3, 28, 32] (let us remind that the domain is here the white matter). Also, the reader can easily verify that this function V coincides with the Riemannian distance to x_0 under the metric $|\cdot|_R$. The explicit Hamiltonian associated to this PDE is

$$H_{AEik}(x, p) = |A_x p|_E - 1 = |p|_R - 1.$$

The control framework [3] also reveals that $f(x, \alpha_x^*) = -\nabla H(x, \nabla u(x))$ where H is the Hamiltonian associated to the PDE (3) and ∇u is the gradient of its solution. Finally, the control formulation of the problem directly yields our numerical method, which we report in sections 4.2 and 4.3. For practical purposes, we will adopt either interpretation depending on the situation and exploit their complementary benefits.

3 Connectivity Measures

We start by pointing out that, for a fixed point x_0 and any point x , the geodesic γ_x (associated to the metric given by the tensors) connecting x to x_0 always exists. If x is connected to x_0 by a white matter fiber then the associated geodesic γ_x coincides with the fiber. Nevertheless, for any x , the associated geodesic γ_x does not necessarily coincide with a fiber. Also, in order to reach our goal (reconstruction of the white matter fiber) we then need to be able to trace the geodesics and to evaluate if a point is potentially connected to x_0 .

In this section, we propose a score to measure the expectation that a given geodesic truly represents the connection of a point x with x_0 . By computing statistical maps of this measure for all points x in the brain, we can then determine which points are likely to be connected to x_0 and then trace the fibers. In section 4 we propose an original numerical scheme based on Fast Marching methods (FMM) to efficiently compute these maps.

Let us fix a point of interest $x_0 \in \bar{\Omega}$ and let us consider the PDE/control/Riemannian problem associated with DTI. In section 2, we show that, $\forall x \in \Omega$, the optimal dynamics f_x^* coincides with the derivatives of the geodesics $\gamma'(t)$ at x and that they are in the Riemannian unit ball $B_R(0, 1)$ which is also the set $\{A_x q, q \in B_E(0, 1)\}$.

So, for a fixed point x (and a fixed tensor D_x), the larger the Euclidian norm of f_x^* , the more confident we are in the local direction of the geodesic. Following this idea, we then define a general (local) confidence measure:

$$\mathcal{C}(x) = \sqrt{f_x^{*T} D_x^\alpha f_x^*},$$

α being in \mathbb{R} . In addition to being intuitive, this measure inherits the robustness to noise of the optimal dynamics. It also exploits the full information provided by the diffusion tensor. Finally, it does not penalize any direction in case of isotropy. Let us now discuss the possible values of α : if $\alpha = -1$, we get $\mathcal{C}(x) = 1, \forall x \in \bar{\Omega}$. This simply means that, when we use the Riemannian metric given by the inverse of the diffusion tensor, all the geodesics are equivalent. On the contrary, when $\alpha = 0$, we have $\mathcal{C}(x) = |f_x^*|_E$ and we claim that it is a natural local measure of connectivity since this measures the *speed* of propagation at x . Finally, when $\alpha \rightarrow \infty$, this boils down to considering

the alignment of the optimal dynamics with the local major eigenvector. This was used in [24] but it is highly sensitive to isotropic areas where, by definition, the major eigenvector is undefined.

From this local connectivity measure, we can define global information from its statistics (mean and standard deviation) along the optimal trajectory:

$$\mu(x) = \langle \mathcal{C}(x) \rangle = \frac{1}{\tau_x^*} \int_0^{\tau_x^*} \mathcal{C}(\xi_x^*(t)) dt,$$

$$\sigma(x) = \sqrt{\langle \mathcal{C}(x)^2 \rangle - \langle \mathcal{C}(x) \rangle^2}.$$

where τ_x^* is the length of the optimal trajectory ξ_x^* . We should point out that, since $|\xi_x^{*'}|_R = 1$, this length (i.e. the geodesic distance between the curve endpoints x_0 and x) coincides with the arrival time T_{x,x_0} introduced in section 2.

A point x connected to x_0 by a white matter fiber will have a large value for $\mu(x)$ and a small standard variation $\sigma(x)$. The choice of using the mean instead of just integrating along the trajectories allows the comparison of two points x and y which are located at different distance from x_0 , i.e. s.t. $\tau_x^* \neq \tau_y^*$. Although the mean value of the connectivity may be sufficient to discriminate likely fibers, the variance of this quantity may also be of great help since an ideal fiber would exhibit a high coherence of $\mathcal{C}(x)$ along its trajectory.

Remark 1.

To compute the optimal dynamics, we need to compute also the geodesic distance, which in fact is equal to τ_x^* . In practice, we just need to compute

$$\mathcal{R}(x) = \int_0^{\tau_x^*} \mathcal{C}(\xi_x^*(t)) dt,$$

and

$$\mathcal{S}(x) = \int_0^{\tau_x^*} \mathcal{C}(\xi_x^*(t))^2 dt.$$

The values of $\mu(x)$ and $\sigma(x)$ are then derived immediately by using the previous value τ_x^* .

4 A Fast Numerical Algorithm

4.1 Related Work and Contributions

To the best of our knowledge, there is no algorithm to compute *directly* the geodesics or a fiber connectivity confidence map to a point x from DTI data. All the methods recovering white matter fibers proceed by implementing successively the following four steps:

1. Computation of the distance function to x ;
2. Extraction of the gradients of the distance function;

3. Estimation of the optimal dynamics from the gradients of the distance function;
4. Tracing of the geodesics from the computed directions. This step needs in particular an interpolation of the derivatives of the geodesics.

Some slight variants are proposed in the literature (see [10, 16] and references therein). For example, in the particular case of the isotropic Eikonal equation (where the optimal dynamics coincide with the gradient of the distance function), [16] suggests not to compute the gradients for all voxels and later interpolate them, but rather to directly compute the interpolated gradients from the distance function.

We wish to emphasize that the explicit tracing of the geodesics is a prerequisite to all the previous methods for computing connectivity confidence measures which in fact consist in the integration of a local criterion along the entire geodesic during the geodesics tracing step. Thus, the estimation of a complete map of connectivity measures needs to explicitly trace all the geodesics starting from all the points of the map. This approach is rather computationally intensive.

The numerical method we propose here for computing the confidence measures does not need to trace any geodesic. The confidence measure map is a direct output of our algorithm. It simultaneously and consistently computes the (geodesic) distance function, the optimal dynamics and the confidence measures.

The methods of the type “Fast Marching” [34, 30, 31, 27] are “one-pass” methods allowing to solve numerically partial differential equations of the type (3). Based on a causality principle, the Fast Marching Methods (FMM) stand in contrast to iterative methods (see for example [29, 33] and more specifically [15] in our field) which iteratively update the approximations of the solution by using paths that do not depend on the data. The idea of the FMM consists in computing the solution of the PDE in proportion as a front propagates along the optimal trajectories. Our algorithm extends the classical FMM [34, 30, 31, 27] by computing and returning in addition the optimal dynamics and the connectivity confidence measures. The consistency of our results relies on the fact that for all the computations we use the same (optimal) simplex.

Remark 2.

- 1) All the quantities we compute are essential: The optimal dynamics are necessary in order to trace the geodesic, which in turn is useful for the visualisation of the fibers. Even if the result of the computation of the (geodesic) distance is not required for tracing the geodesic, it is essential for obtaining the final measures (expectation and standard deviation) we use in practice to estimate the connectivity confidence.
- 2) Our method is a “one pass method” based on front propagation. An important consequence is that we do not need to wait for the complete computation of the distance function on the whole domain to be able to exploit it for computing the connectivity measures. Also, if at any time the process stops, all the values already computed are valid approximations, unlike other iterative techniques.

In the sequel, we describe our global algorithm and then the implementation of each specific step.

4.2 Global Algorithm

As in the classical ‘‘Fast Marching Method’’ [30, 31, 27], the grid points are divided into the three classes: *Accepted*, *Considered*, *Far*. Below U , f , R and S are respectively the approximations of the (geodesic) distance function, the optimal dynamics f_x^* , \mathcal{R} and \mathcal{S} (defined in section 3). x_0 is the interest point. The algorithm is then the following:

Algorithm 1 Fast Marching algorithm for the computation of U , f , R and S

- 1: Start with all the grid points in *Far*.
 - 2: Move x_0 and the grid points on the boundary $\partial\Omega$ to *Accepted*. Set $U(x_0) = 0$ and $U(x) = +\infty$ (*FLT_MAX* in practice) for all $x \in \partial\Omega$.
 - 3: Move all the grid points adjacent to the *Accepted* points into *Considered* and for such points x , evaluate $U(x)$ by using the update scheme (4) and modify the associated optimal dynamics to $f(x)$; see section 4.3.
 - 4: Find the *Considered* point \tilde{x} with the smallest value $U(x)$. Move \tilde{x} from *Considered* to *Accepted*. Compute and assign $R(\tilde{x})$ and $S(\tilde{x})$, see section 4.4.
 - 5: Move from *Far* into *Considered*, all the *Far* points which are adjacent to \tilde{x} .
 - 6: Re-evaluate $U(x)$ and the associated dynamics $f(x)$ for all the *Considered* points adjacent to \tilde{x} , see section 4.3.
 - 7: If the set *Considered* points is not empty, return to step 4.
-

4.3 Distance and Optimal Dynamics Computation

Here, we focus on the implementation of the updating step returning the approximation of the distance function and the optimal dynamics. Following [27], we use the scheme

$$S(\rho, x, t, u) = \sup_{a \in A} \{-f(x, a) \cdot P_{s_1(x,a), \dots, s_N(x,a)} - l(x, a)\} \quad (4)$$

where $[P_{s_1, \dots, s_N}]_i = \frac{t - u(x + s_i h_i e_i)}{-s_i h_i}$, $s_i(x, a) = \text{sign}(f_i(x, a))$, h_i denotes the grid size in the i^{th} direction and $\{e_i\}$ is the canonical basis of \mathbb{R}^N . In our case, $N = 3$.

Basically, this scheme is obtained by replacing ∇u by P_{s_1, \dots, s_N} in equation (3) and by choosing the simplex (i.e. (s_1, \dots, s_N)) which contains the dynamics of the optimal control. Moreover, we take advantage of this in order to obtain *simultaneously and consistently* the approximations of the geodesic distance function and of the optimal dynamics.

4.3.1 Separation and choice of the good simplex

Let us fix $x \in \Omega$. The updating step consists in computing the value we want to assign to $U(x)$ from the values $U(x \pm s_i h_i e_i)$. The update value for $U(x)$ is the solution of the equation $S(\rho, x, t, u) = 0$ (equation in t), i.e.

$$\max_{s \in \{\pm 1\}^N} \sup_{a \in A_s} \{-f(x, a) \cdot P_{x, s, U}(t) - l(x, a)\} = 0$$

where we note $s = (s_1, \dots, s_N) \in \{\pm 1\}^N$, $[P_{x,s,U}(t)]_i = \frac{t - U(x + s_i h_i e_i)}{-s_i h_i}$ and

$$A_s = \{a \in A \mid \forall i = 1..N, s_i(x, a) = s_i\}.$$

Now, for all $s \in \{\pm 1\}^N$, let us denote

$$G_s(t) = \sup_{a \in A_s} \{-f(x, a) \cdot P_{x,s,U}(t) - l(x, a)\} \quad (5)$$

and t_s , the solution of the equation (in t) $G_s(t) = 0$. Since $G_s(t)$ is increasing with respect to t , the solution of $\max_s G_s(t) = 0$ is $t_0 = \min_{s \in \{\pm 1\}^N} t_s$. Hence, the implementation of the update step is reduced to the computation of the 2^N solutions t_s and, finally, to the choice of the smallest one. We thus choose here the “good” simplex. We call it the *optimal simplex*. In other respects, when we compute t_s , we also compute $f_s = f(x, a_s)$, where $a_s \in A_s$ is the optimal control of (5) (see subsection 4.3.2). We can then associate to t_0 the optimal dynamics $f_0 = f_s$ where s is the optimal simplex.

4.3.2 Computation of t_s and of the associated dynamics

Now let us fix $s = (s_1, \dots, s_N) \in \{\pm 1\}^N$. If we denote

$$g_s(a, t) = -f(x, a) \cdot P_{x,s,U}(t) - l(x, a),$$

then t_s is the solution of

$$\sup_{a \in A_s} g_s(a, t) = 0. \quad (6)$$

By continuity of $f(x, \cdot)$, A_s is a closed subset of \mathbb{R}^M . Let a_s in A_s be the *optimal control* of (6). We then have two cases:

1. $\forall k \in [1..N]$, $f_k(x, a_s) \neq 0$ (in other words $a_s \in \text{Interior}(A_s)$): One can prove that this is equivalent to: t_s is the solution of the equation $H(x, P_{x,s,U}(t)) = 0$ with the associated optimal control¹ in A_s .
2. $\exists k \in [1..N]$ such that $f_k(x, a_s) = 0$: In this case, $t_s = \min t_s^i$, where for each $i \in [1..N]$, t_s^i is the solution of the equation in t : $\sup_{a \in A_s^{i+}} g_s(a, t) = 0$ where $A_s^{i+} = A_s^k \cap A_s$ and $A_s^k = \{a \in A \mid f_i(x, a) = 0\}$.

In practice, we first compute the roots t_s of $H(x, P_{x,s,U}(t)) = 0$. We then test if the optimal control $a_s \in A_s$ (basically it is in A). To do that, we just have to estimate

$$f(x, a_s) = -\nabla H(x, P_{x,s,U}(t_s))$$

and to verify that $\forall k, \text{sign}(f_k(x, a_s)) = s_k$. In particular, this test does not require the knowledge of the optimal control a_i and directly provides the associated optimal dynamics. If all the signs are

¹i.e. the optimal control of $\sup_{a \in A} \{-f(x, a) \cdot P_{x,s,U}(t) - l(x, a)\} = 0$. This optimal control can be anywhere in the whole set A .

correct, we have found our solution and we stop here. Otherwise, we have to compute the solutions t_s^i . To achieve this goal, we can make

$$H_s^i(x, p) \stackrel{\text{def}}{=} \sup_{a \in A_s^k} \{-f(x, a) \cdot p - l(X, a)\} = 0$$

explicit and deal with H_s^i in the same way we have dealt with H . To make H_s^i explicit we use the Legendre Transform [27].

4.3.3 Details for the 3D-anisotropic eikonal equation

Here we detail the successive Hamiltonians necessary to the implementation the method described in the previous section in the case of the 3D-anisotropic Eikonal Equation. Because of space, we cannot report all the calculations.

Let us remind that for any Hamiltonian $H(x, p)$, we call the *Legendre Transform* the function H^* defined by

$$H^*(x, a) = \sup_{p \in \text{Dom}(H(x, \cdot))} \{p \cdot a - H(x, p)\} \leq +\infty$$

see for example [12, 26]. For simplicity, we denote below the Hamiltonian H_{aEik} by H . We have

$$H_i(x, p) \stackrel{\text{def}}{=} \sup_{\substack{a \in \mathbb{R}^3 \\ a_i = 0}} \{a \cdot p - H^*(x, a)\} = \tilde{p}_t^{iT} ([D_x^{-1}]^i)^{-1} \tilde{p}_t^i - 1,$$

$$H_{ij}(x, p) \stackrel{\text{def}}{=} \sup_{\substack{a \in \mathbb{R}^3 \\ a_i = 0, a_j = 0, i \neq j}} \{a \cdot p - H^*(x, a)\} = \frac{p_{tk}^2}{(D_x^{-1})_{k,k}} - 1,$$

where $\tilde{p}_t^i = (p_{t_1}, \dots, p_{t_{i-1}}, p_{t_{i+1}}, \dots, p_{t_n})$, and $[D_x^{-1}]^i$ is the matrix D_x^{-1} without the i^{th} row and i^{th} column. In practice our method boils down to resolving basic second order equations and to testing some signs.

4.4 Connectivity Measures Computation

In this section we detail how to compute the connectivity measure $\mathcal{R}(\tilde{x})$ at the step 4 of our global algorithm. At this stage, we already know the optimal dynamics $f_{\tilde{x}}^*$, the optimal simplex $(\tilde{x}, x_1, x_2, x_3)$ (we denote $x_i = \tilde{x} + s_i(\tilde{x})h_i e_i$ where $s_i(\tilde{x})$ is the sign of the i^{th} component of $f_{\tilde{x}}^*$ and $h_1 \times h_2 \times h_3$ is the size of the voxels) and the values $\mathcal{R}(x_i)$ for $i = 1..3$.

Let y be the intersection of the optimal trajectory with the front. By assuming that the trajectory is locally affine, we have: $y = \tilde{x} + \tau f_{\tilde{x}}^*$ where τ is the time for the trajectory to reach the front, see figure 1(a). As in [25], we can prove that

$$\tau = 1 / \sum_{i=1..3} q_i$$

where q_i is the absolute value of the i^{th} component of $f_{\tilde{x}}^*$ divided by h_i . By assuming that \mathcal{R} is locally affine, we have [25]

$$\mathcal{R}(y) = \sum_{i=1}^3 \tau q_i \mathcal{R}(x_i).$$

Thus by noting that

$$\mathcal{R}(\tilde{x}) = \mathcal{R}(y) + \int_0^\tau \mathcal{C}(\xi_{\tilde{x}}^*(t)) dt,$$

we obtain

$$\mathcal{R}(\tilde{x}) \simeq \sum_{i=1}^3 \tau q_i \mathcal{R}(x_i) + \tau \mathcal{C}(\tilde{x}). \quad (7)$$

Remark 3.

- 1) The approximation of $\mathcal{S}(\tilde{x})$ required for the computation of the standard deviation $\sigma(\tilde{x})$ is obtained exactly in the same way. We just have to replace \mathcal{C} by \mathcal{C}^2 in equation (7).
- 2) This scheme can also be obtained by discretizing the equation $\langle \nabla_E \mathcal{R}(x), f_x^* \rangle_E = \mathcal{C}(x)$ (obtained by evaluating $\lim_{\varepsilon \rightarrow 0} \frac{\mathcal{R}(x+\varepsilon f_x^*) - \mathcal{R}(x)}{\varepsilon}$) and by slightly modifying the scheme proposed by [1] for solving a similar equation.

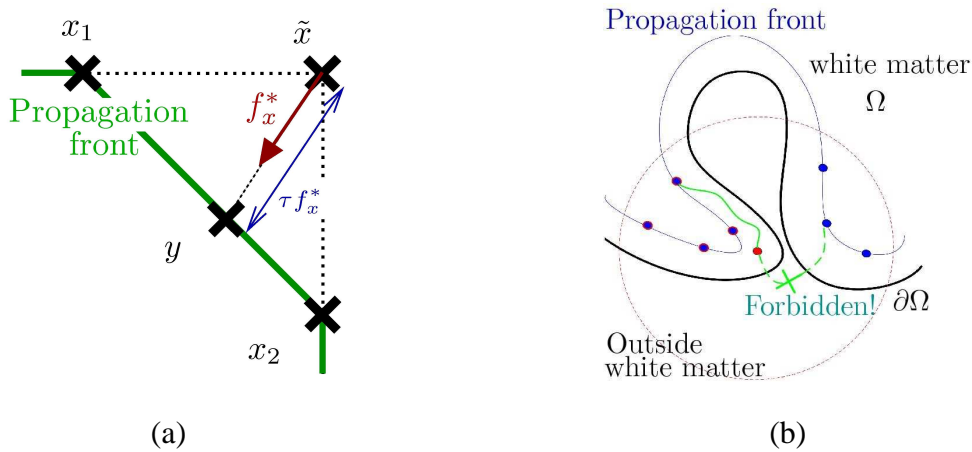


Figure 1: (a) Approximation of the geodesic and localization of y , (b) Depiction of the topological problem in a convoluted area of the white matter

5 Experimental Results

5.1 Challenging Computational Issues

The nature of the problem we are trying to solve raises two major computational difficulties which, to our knowledge, are not very well dealt with in the literature.

5.1.1 Handling the white matter convoluted geometry

First of all, as presented in figure 2 and detailed in figure 1(b), solving the anisotropic eikonal equation within a convoluted domain such as the brain white matter is necessary and complicated. Indeed, the connections we are looking for are defined between cortical areas or between cortical areas and the basal ganglia (a collection of subcortical nuclei deeply included in the white matter). In other words, we are essentially interested in pathways linking together parts of the domain boundary.

In figure 2, the geodesic distance to the blue cross in image (b) (i.e. x_0) was computed, for the DTI data presented in image (a) and within the mask outlined in red in image (b). Its isovalues (in the range $[0, 1500]$) are depicted by the yellow lines in images (c) and (d). With a level set implementation such as the one proposed by Lenglet et al. [18], the front diffuses through the CSF and directly connects the right hemisphere. This is anatomically incorrect since the fibers starting from the blue cross (located in the V1 visual area) go through the corpus callosum (CC) to reach the other hemisphere. Our method correctly estimates the distance since, by definition, it ignores all the locations outside the mask.

This kind of difficulties is also encountered with the Ordered Upwind Method (OUM) recently proposed by Sethian and Vladimirsky [31]. The OUM is a numerical method of type FMM which uses enlarged neighborhoods. The more anisotropic the tensor, the larger the neighborhood. In addition to increasing the computation time, Sethian and Vladimirsky’s method explicitly authorizes this type of topological error by allowing the trajectories to step outside the mask and to directly connect any nearby voxel located on the front. Figure 1(b) illustrates this potential problem. The scheme we use here only uses nearest neighbors (six nearest neighbors in 3D). Our method is not sensitive to this problem and always respects the topology of the mask.

5.1.2 Robust estimation of the optimal dynamics

The second issue is related to the robustness of the optimal dynamics (i.e. the geodesics tangent vectors) computation. Indeed, all the existing methods need to explicitly compute the derivatives of the distance function. This is well-known to be sensitive to noise, especially on the boundaries where the discretization of the differential needs to be adapted. We present, in figure 3, a comparison of the vector fields obtained by the method proposed in [18] (top row) and by our approach (bottom row) on a 3D synthetic DTI dataset (see image (a)). The origin of the distance function is located at the center of region B (see image (b)).

5.2 Fast and Robust Anatomical Connectivity Measure

In the following, we illustrate our method by computing the quantities μ and σ , introduced in section 3, as well as the geodesics associated to the highest connectivity measure. This is done on the synthetic tensor field of figure 3 as well as in the splenium (posterior part) of the corpus callosum for the real dataset of figure 2.

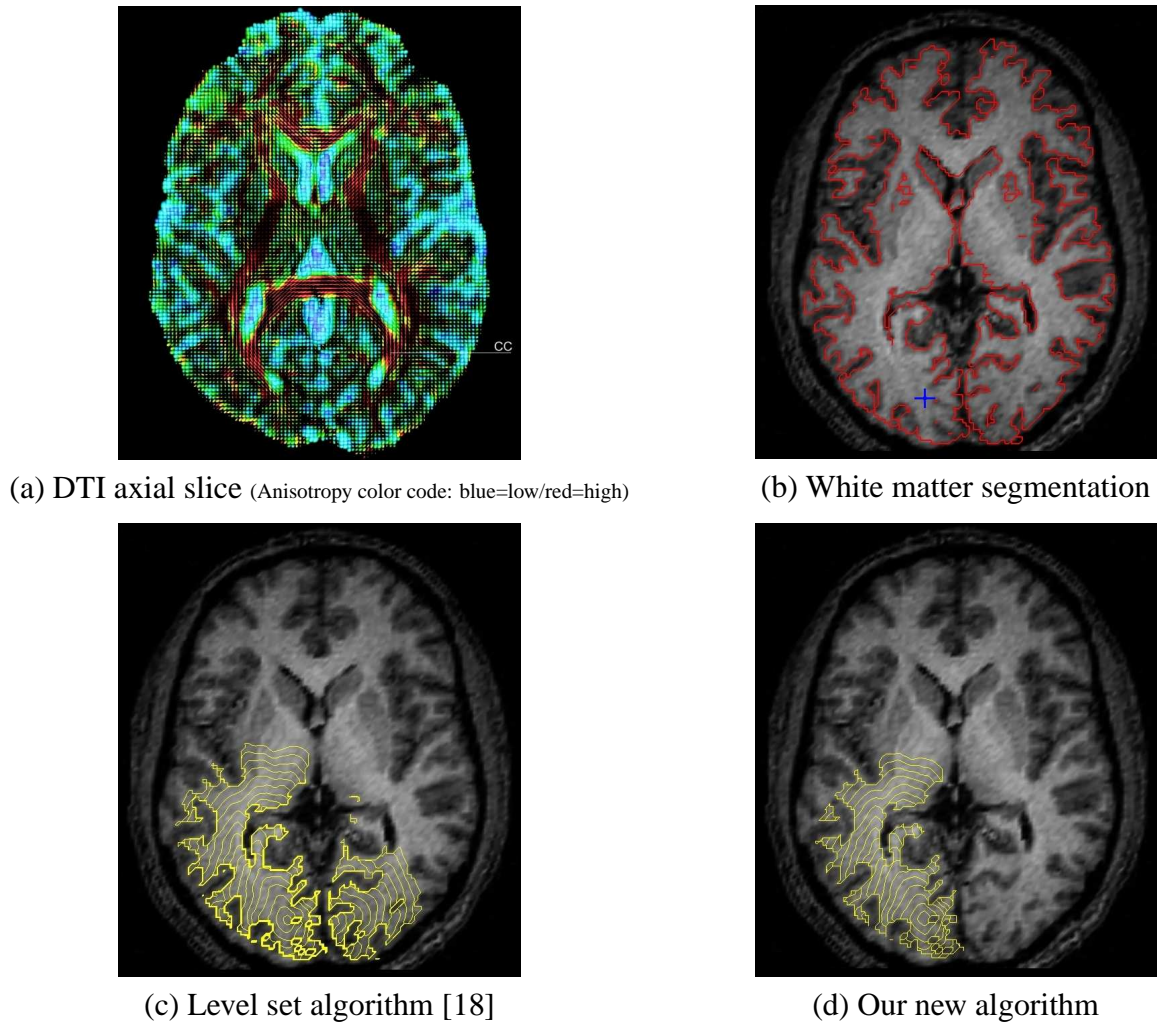


Figure 2: Topological inconsistency in the occipital cortex.

5.2.1 Data acquisition

Diffusion weighted images were acquired on a 3 Tesla Bruker scanner at the *Centre IRMf de Marseille*, France. We used 12 diffusion gradient directions and a b -value of 1000 s/mm^2 . Acquisitions were repeated 8 times for each direction in order to ensure a good signal-to-noise ratio. Voxel size was $2 \times 2 \times 2 \text{ mm}^3$ and diffusion tensors were estimated by the robust gradient descent algorithm proposed in [19]. An axial slice of the resulting DT image is presented in figure 2(a).

5.2.2 Computational efficiency

PDE methods for brain connectivity mapping such as [21, 24, 18, 15, 9] have the great advantage to yield connectivity information for a point of interest x_0 to the rest of the brain by exploiting the full information of the diffusion tensor. They are however in general quite time consuming and must be iteratively applied to all the voxels of the functional regions of interest, which can contain

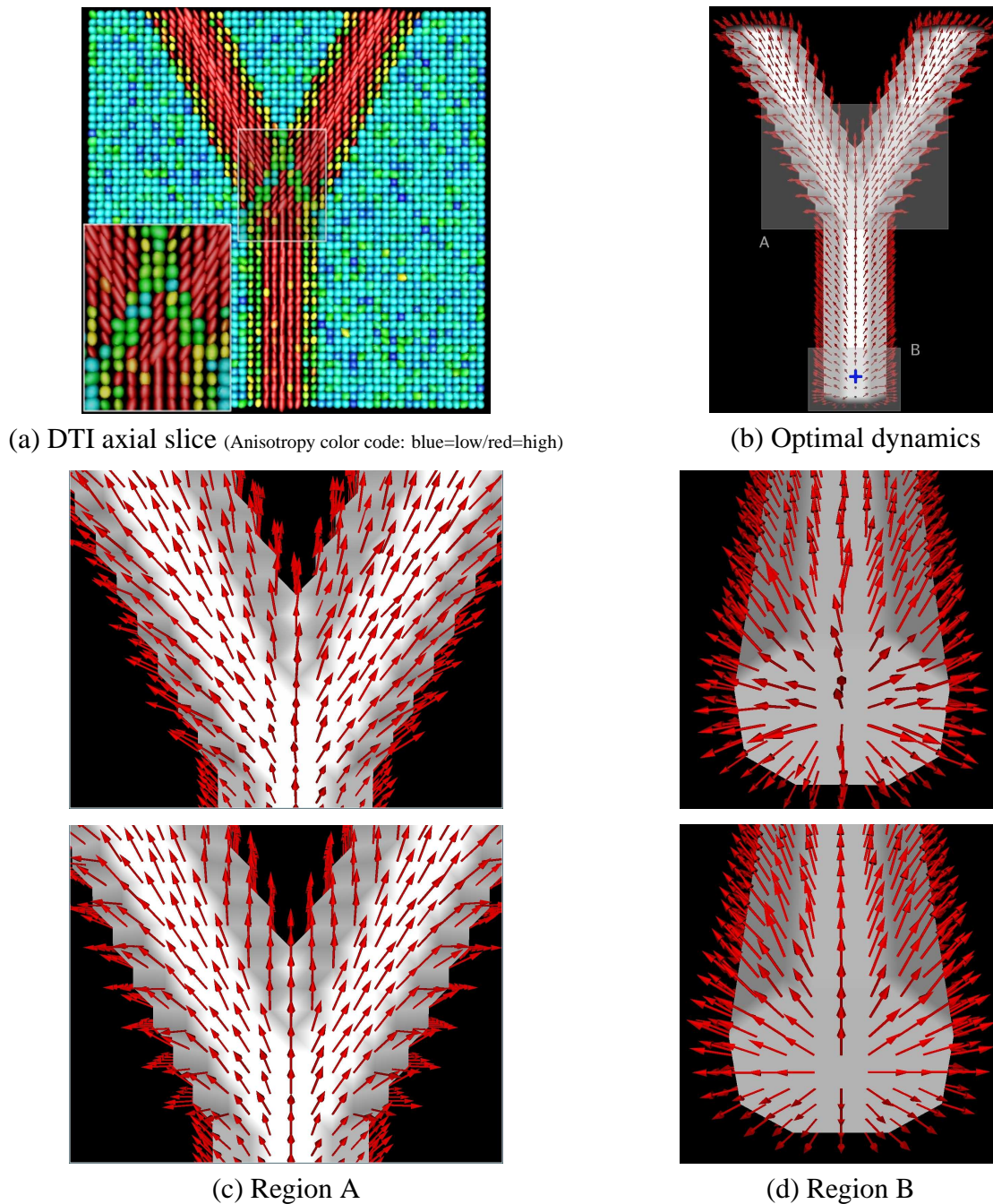


Figure 3: Optimal dynamics estimation by differentiation of the distance [(c-d) Top] and by our direct method [(c-d) Bottom].

hundreds or thousands of points.

By comparison with the methods presented in [15] and [18], our algorithm achieves a dramatic improvement in computational speed. For the geodesic distance computation, Jackowski et al. reported a convergence time of about **7 minutes** for their iterative sweeping method for a $128 \times$

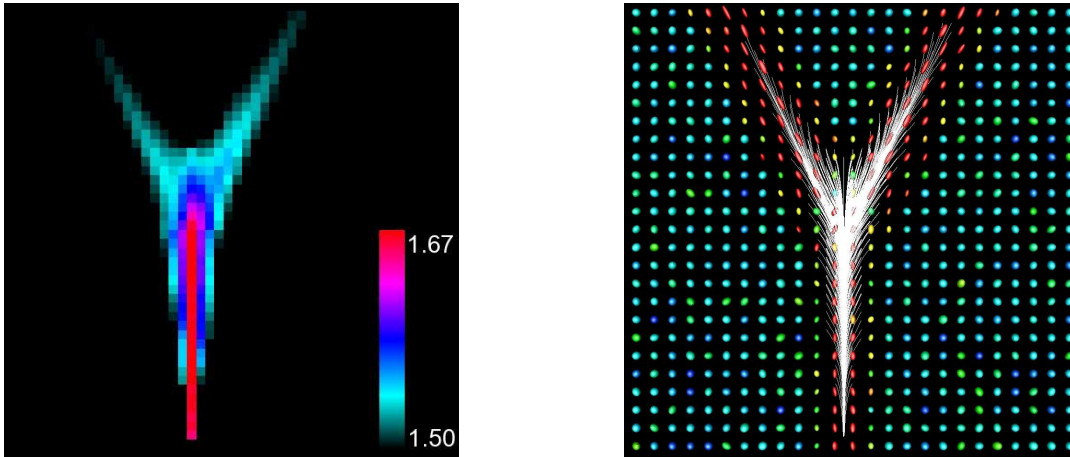


Figure 4: Synthetic dataset: [Left] Axial slice of the map μ , [Right] Most likely connections.

128 × 40 DTI dataset on a 1.7 GHz Intel Pentium Xeon with 1.5 Gb of RAM. We also tested the level set formulation proposed by Lenglet et al. It required about **20 minutes** for a 128 × 128 × 58 DTI dataset on a 1.7 GHz Intel Pentium M with 1 Gb of RAM.

The computation of the geodesics, together with the evaluation of the statistics of $\mathcal{C}(x)$, is itself a time-consuming task since for each curve, we need to explicitly propagate through the tangent vectors field using, for instance, a 4th order Runge-Kutta integration scheme. In [15], no time is given for the computation of the 14,952 fibers of interest. However, on our data and for 135,029 voxels inside the white matter mask, it took approximately **30 minutes** on the same computer than the one used for the distance computation. All these computations (distance, vector field and connectivity measures) take about **7 seconds** with our method.

5.2.3 Performance of the connectivity measure

We now demonstrate how the statistics of the quantity $\mathcal{C}(x)$ can be used to evaluate the degree of connectivity of pairs of voxels. First of all, we use the synthetic dataset of figure 3. The point of interest x_0 is again located at the center of region B (see image (b)). Figure 4 [Left] presents an axial slice of the thresholded map μ which is consistent with the DT image since we can see that μ is higher along the centerline of the Y shape where the tensors are more anisotropic. Moreover, the right branch is clearly more connected to the origin. This is due to the asymmetry imposed by the tensor field in the diverging region (see figure 3 (a)). In figure 4 [Right], we show the geodesics computed from the 873 voxels with values of μ in the range [1.5, 1.67], i.e. the top 10% most likely connected voxels. Finally, we consider the real dataset of figure 5. The origin is located in the middle of the splenium of the corpus callosum. A first threshold is applied on the map σ in order to keep only coherent fibers. This yields a binary mask (threshold value: 0.0056) which is applied to the map μ . As previously, we then threshold this map to preserve only the top 10% most likely connected voxels, with values of μ in the range [0.0335, 0.0380]. This yields 2561 fibers that are consistent with neuro-anatomical knowledge.

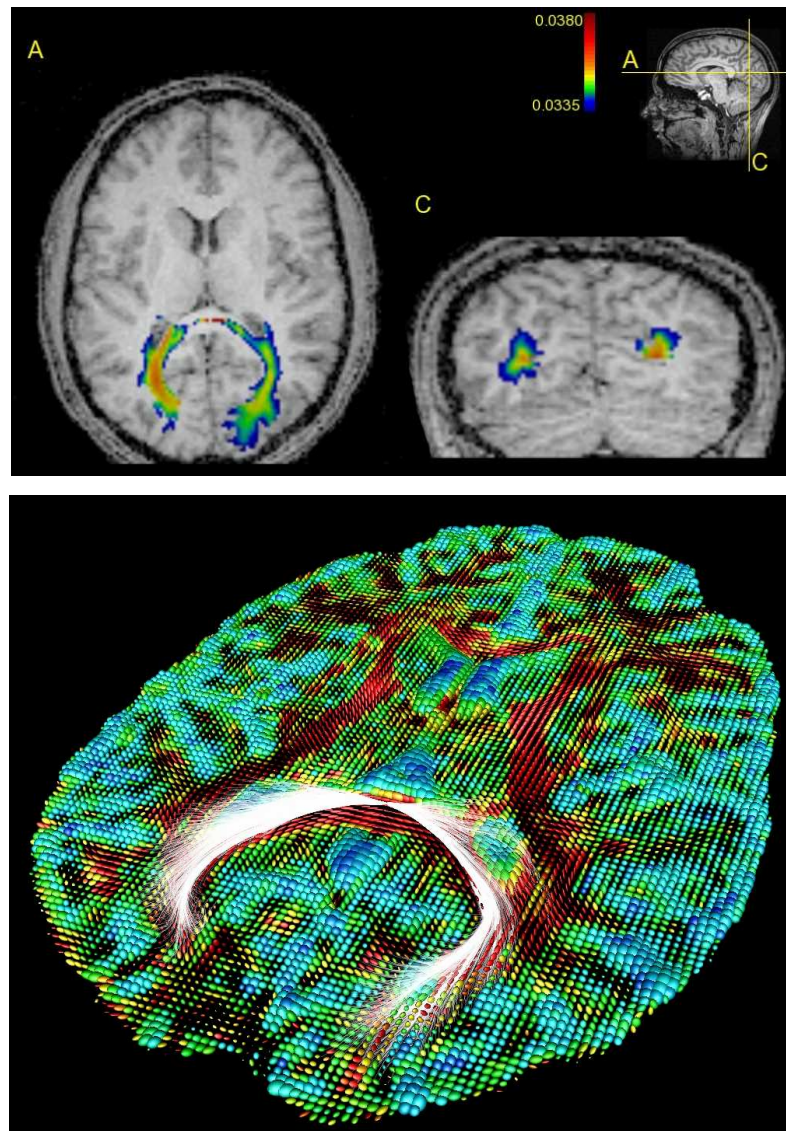


Figure 5: Real dataset: [Top] Axial and coronal slices of the map μ , [Bottom] Most likely connections (Anisotropy color code: blue=low/red=high).

6 Conclusion

We have introduced a general local connectivity measure and experimentally demonstrated its relevance on real data sets. Exploiting both an optimal control and a Riemannian interpretation, we achieved a number of improvements over existing methods. We proposed a fast algorithm that reduces CPU time by 2 or 3 orders of magnitude relatively to existing work. Our algorithm is numerically stable and efficient, since it simultaneously computes the distance function, the optimal dynamics and the statistics of our local connectivity measure from the DT images. Finally we showed that our method overcomes numerical limitations that cause existing algorithms to fail

in highly convoluted regions. The C++ implementation of our **GCM** algorithm will be soon freely distributed on the web.

Acknowledgments

This research was partially supported by grants NIH U54 RR021813, ONR N00014-03-1-0850, AFOSR F49620-03-1-0095, ACI Obs-Cerv and the Région Provence-Alpes-Côte d'Azur. The authors would like to thank J.L. Anton, M. Roth and N. Wotawa for the human brain DTI dataset used in this paper.

References

- [1] D. Adalsteinsson and J.A. Sethian. The fast construction of extension velocities in level set methods. *Journal of Computational Physics*, 148(1):2–22, 1999.
- [2] A.L. Alexander, K.M. Hasan, M. Lazar, J.S. Tsuruda, and D.L. Parker. Analysis of partial volume effects in diffusion-tensor mri. *Magnetic Resonance in Medicine*, 45(5):770–780, 2001.
- [3] M. Bardi and I. Capuzzo-Dolcetta. *Optimal control and viscosity solutions of HJB equations*. Birkhauser, 1997.
- [4] P. Basser, J. Mattiello, and D. le Bihan. MR diffusion tensor spectroscopy and imaging. *Biophysical Journal*, 66:259–267, 1994.
- [5] P.J. Basser, S. Pajevic, C. Pierpaoli, J. Duda, and A. Aldroubi. In vivo fiber tractography using DT-MRI data. *Magn. Res. Med.*, 44:625–632, 2000.
- [6] T. Behrens, M. Woolrich, M. Jenkinson, H. Johansen-Berg, R. Nunes, S. Clare, P. Matthwes, J. Brady, and S. Smith. Characterization and propagation of uncertainty in diffusion-weighted MR images. *Magnetic Resonance in Medicine*, 50:1077–1088, 2003.
- [7] D. le Bihan, E. Breton, D. Lallemand, P. Grenier, E. Cabanis, and M. Laval-Jeantet. MR imaging of intravoxel incoherent motions: Application to diffusion and perfusion in neurologic disorders. *Radiology*, 401–407, 1986.
- [8] M. Bjornemo, A. Brun, R. Kikinis, and C.F. Westin. Regularized stochastic white matter tractography using diffusion tensor MRI. In *Proceedings of MICCAI*, 435–442, 2002.
- [9] S.W. Campbell, K. Siddiqi, V.V. Rymar, A.F. Sadikot, and G.B. Pike. Flow-based fiber tracking with diffusion tensor q-ball data: Validation and comparison to principal diffusion direction techniques. *NeuroImage*, 27(4):725–736, October 2005.
- [10] L. Cohen. Minimal paths and fast marching methods for image analysis. In *Mathematical Models in Computer Vision: The Handbook*, Chapter 7. Springer, 2005.

-
- [11] M. P. DoCarmo. *Riemannian Geometry*. Birkhäuser, 1992.
- [12] I. Ekeland and R. Temam. *Analyse Convexe et Problèmes Variationnels*. Etudes mathématiques. Dunod, Gauthier-Villars, 1974.
- [13] O. Friman and C.F. Westin. Uncertainty in white matter fiber tractography. In *Proceedings of MICCAI*, 107–114, 2005.
- [14] P. Hagmann, J.P. Thiran, L. Jonasson, P. Vandergheynst, S. Clarke, P. Maeder, and R. Meuli. DTI mapping of human brain connectivity: Statistical fiber tracking and virtual dissection. *NeuroImage*, 19:545–554, 2003.
- [15] M. Jackowski, C.Y. Kao, M. Qiu, R.T. Constable, and L.H. Staib. White matter tractography by anisotropic wavefront evolution and diffusion tensors imaging. *Medical Image Analysis*, 9:427–440, 2005.
- [16] R. Kimmel and J. A. Sethian. Computing Geodesic Paths on Manifolds. *Proceedings of the National Academy of Science*, 95(15):8431–8435, 1998.
- [17] M. Lazar, D.M. Weinstein, J.S. Tsuruda, K.M. Hasan, K. Arfanakis, M.E. Meyerand, B. Badie, H.A. Rowley, V. Haughton, A. Field, and A.L. Alexander. White matter tractography using diffusion tensor deflection. In *HBM*, 18:306–321, 2003.
- [18] C. Lenglet, R. Deriche, and O. Faugeras. Inferring white matter geometry from diffusion tensor MRI: Application to connectivity mapping. In *Proceedings of ECCV*, 127–140, 2004.
- [19] C. Lenglet, M. Rousson, R. Deriche, and O. Faugeras. Statistics on the manifold of multivariate normal distributions: Theory and application to Diffusion Tensor MRI. *Journal of Mathematical Imaging and Vision*, (In press) 2006.
- [20] S. Mori, B.J. Crain, V.P. Chacko, and P.C.M. Van Zijl. Three-dimensional tracking of axonal projections in the brain by magnetic resonance imaging. *An. of Neurology*, 45(2):265–269, 1999.
- [21] L. O’Donnell, S. Haker, and C.F. Westin. New approaches to estimation of white matter connectivity in diffusion tensor MRI: Elliptic PDEs and geodesics in a tensor-warped space. In *Proceedings of MICCAI*, 459–466, 2002.
- [22] S. Osher and J.A. Sethian. Fronts propagating with curvature-dependent speed: Algorithms based on Hamilton–Jacobi formulations. *Journal of Computational Physics*, 79(1):12–49, 1988.
- [23] G.J. Parker, H.A. Haroon, and C.A. Wheeler-Kingshott. A framework for a streamline-based probabilistic index of connectivity (pico) using a structural interpretation of MRI diffusion measurements. *Journal of Magnetic Resonance Imaging*, 18(2):242–254, August 2003.

-
- [24] G.J.M. Parker, C.A.M. Wheeler-Kingshott, and G.J. Barker. Estimating distributed anatomical connectivity using fast marching methods and diffusion tensor imaging. *IEEE Transactions on Medical Imaging*, 21(5):505–512, 2002.
- [25] E. Prados, O. Faugeras, and E. Rouy. Shape from shading and viscosity solutions. Research Report 4638, INRIA, 2002.
- [26] E. Prados. Application of the theory of the viscosity solutions to the Shape From Shading problem. Ph.D. Thesis, University of Nice-Sophia Antipolis, 2004.
- [27] E. Prados and S. Soatto. Fast marching method for generic shape from shading. In *Proceedings of VLISM*, 320–331, 2005.
- [28] E. Prados, F. Camilli, and O. Faugeras. A unifying and rigorous Shape From Shading method adapted to realistic data and applications. *Journal of Mathematical Imaging and Vision*, (In press) 2006.
- [29] E. Rouy and A. Tourin. A Viscosity Solutions Approach to Shape-from-Shading. *SIAM Journal of Numerical Analysis*, 29(3):867–884, June 1992.
- [30] J.A. Sethian. A fast marching level set method for monotonically advancing fronts. In *Proceedings of the National Academy of Sciences*, 93:1591–1694, 1996.
- [31] J.A. Sethian and A. Vladimirsky. Ordered upwind methods for static Hamilton–Jacobi equations: Theory and algorithms. *SIAM Journal of Numerical Analysis*, 41(1):325–363, 2003.
- [32] H.M. Soner. Optimal control with state space constraints. *SIAM Journal on Control and Optimization*, 24, part I: 552–562 & part II: 1110–1122, 1986.
- [33] Y.H. Tsai, L.T. Cheng, S. Osher, and H.K. Zhao. Fast sweeping algorithms for a class of Hamilton–Jacobi equations. *SIAM Journal of Numerical Analysis*, 41(2):673–694, 2003.
- [34] J.N. Tsitsiklis. Efficient algorithms for globally optimal trajectories. *IEEE Transactions on Automatic Control*, 40:1528–1538, 1995.
- [35] B. Vemuri, Y. Chen, M. Rao, T. McGraw, T. Mareci, and Z. Wang. Fiber tract mapping from diffusion tensor MRI. In *Proceedings of VLISM*, 81–89, 2001.



Unité de recherche INRIA Sophia Antipolis
2004, route des Lucioles - BP 93 - 06902 Sophia Antipolis Cedex (France)

Unité de recherche INRIA Futurs : Parc Club Orsay Université - ZAC des Vignes
4, rue Jacques Monod - 91893 ORSAY Cedex (France)

Unité de recherche INRIA Lorraine : LORIA, Technopôle de Nancy-Brabois - Campus scientifique
615, rue du Jardin Botanique - BP 101 - 54602 Villers-lès-Nancy Cedex (France)

Unité de recherche INRIA Rennes : IRISA, Campus universitaire de Beaulieu - 35042 Rennes Cedex (France)

Unité de recherche INRIA Rhône-Alpes : 655, avenue de l'Europe - 38334 Montbonnot Saint-Ismier (France)

Unité de recherche INRIA Rocquencourt : Domaine de Voluceau - Rocquencourt - BP 105 - 78153 Le Chesnay Cedex (France)

Éditeur

INRIA - Domaine de Voluceau - Rocquencourt, BP 105 - 78153 Le Chesnay Cedex (France)

<http://www.inria.fr>

ISSN 0249-6399